Composite Structures 286 (2022) 115288

Contents lists available at ScienceDirect

Composite Structures

journal homepage: www.elsevier.com/locate/compstruct

# Influences of elastic foundations on the nonlinear free vibration of composite shells containing carbon nanotubes within shear deformation theory

M. Avey [a,b,c,*], N. Fantuzzi [d], A.H. Sofiyev [a,e,f], N. Kuruoglu [g]

[a] Information Technology Research and Application Center Member of Consultancy Board of ITRAC Center of Istanbul Commerce University, Beyoglu 34445/Istanbul, Turkey
[b] Analytical Information Resources Center of UNEC-Azerbaijan State Economic University, 1001/Baku, Azerbaijan
[c] Division of Mathematics in Graduate School of Education of Usak University, Usak, Turkey
[d] Department of Civil, Chemical, Environmental, and Materials Engineering, University Bologna, Italy
[e] Department of Civil Engineering, Engineering Faculty of Suleyman Demirel University, Isparta, Turkey
[f] Scientific Research Centers for Composition Materials of UNEC-Azerbaijan State Economic University, 1001/Baku, Azerbaijan
[g] Department of Civil Engineering of Faculty of Engineering and Architecture, Istanbul Gelisim University, Istanbul, Turkey

ARTICLE INFO

*Keywords:*
CNT
Nanocomposite shell structures
Nonlinear free vibration
Soils
Shear deformation theory
Nonlinear frequencies

ABSTRACT

In this work, the solution of nonlinear free vibration problem of composite shells structures containing carbon nanotubes (CNTs) resting on elastic soils within shear deformation theory (ST) is presented. After modeling the mechanical properties of nanocomposite shell structures containing CNTs and elastic soils, the basic relations, and governing equations of double curved shell structures within the ST are established considering the geometric nonlinearity. The frequencies of nonlinear and linear free vibrations and their ratios for inhomogeneous nanocomposite structures on the soils within the ST are obtained using perturbation method for the first time. After checking the methodology of the research, the effects of soils, nonlinearity, shear strains and patterns of CNT on the frequency-amplitude dependence of nanocomposite shell structures for various geometric parameters are carried out.

## 1. Introduction

One of the promising aspects of contemporary technology to improve mechanical properties of materials is the use of various nanoscale structures. In this sense, strengthening polymers with nanotubes makes them effective load-bearing composites for structural elements of space, machine building, automotive and other engineering applications. One of most effective nano materials is CNTs, which have recently attracted the attention of researchers because of their unique properties in terms of durability, thermal stability, and electrical conductivity A fundamental understanding of the mechanical properties of CNTs, such as Young's modulus, strength, and shear deformation, makes it possible to develop their technological aspects [1–5]. CNTs have great potential to improve the properties of various structures. Many studies have shown that carbon nanotubes can be an effective tool to alter the strength of polymer composite materials [6–10], especially the ones based on epoxy resins used in aircraft construction. Detailed information about the physics, concept, fabrication, and applications of nanocomposites is presented in the refs [11,12].

The properties that contemporary industries expect from composite materials are high strength, formability, electrical properties, corrosion and chemical resistance, and vibration damping. These requirements aroused the interest of researchers in the analysis of nonlinear vibrations of nanocomposite structures containing carbon nanotubes. The first attempt to solve the nonlinear vibration problem of nanocomposite shells started with the study of Shen and Xiang [13]. Based on the models considered for evaluating the mechanical properties of the nanocomposite used in that study, the nonlinear vibration problems of various structural elements were solved by different approaches and methods without considering the effect on an elastic foundation [14–25].

Advances in technology facilitate the daily production of new

* Corresponding author.
*E-mail addresses:* mahmureavey@gmail.com (M. Avey), nicholas.fantuzzi@unibo.it (N. Fantuzzi), abdullahavey@sdu.edu.tr (A.H. Sofiyev), nkuruoglu@gelisim.edu.tr (N. Kuruoglu).

https://doi.org/10.1016/j.compstruct.2022.115288
Received 15 September 2021; Received in revised form 28 November 2021; Accepted 22 January 2022
Available online 29 January 2022

artificial materials. This aspect greatly expands the field of application of structural elements made of artificial materials and facilitates the use of such structural elements in various environments. Among these applications, the interaction of structural elements with the ground becomes more prominent in practice. Soils, in which structural elements are in contact, are usually modeled as one- and two-parameter foundations. The Pasternak foundation model (two-parameter foundation model) is a widely used model for describing the mechanical behavior of soils. This two-parameter foundation model is created by placing a very thin layer of low thickness on the free ends of the parallel springs that make up the Winkler soil model (one-parameter foundation model) [26,27].

Since nanocomposites are also used in civil and mechanical engineering (e.g., at nuclear power plants, etc.), it is necessary to investigate the combined effects of heterogeneity and elastic foundations on the frequency-amplitude dependence caused by dynamic loads in nanocomposite structural elements. In the literature, most nonlinear dynamic problems related to the interaction of nanocomposite structures with soil have been solved using numerical methods. Some of the studies on this subject are devoted to the analytical solution of either linear or nonlinear vibration problems in the framework of classical shell theory. Tornabene et al. [28] used differential quadrature method to investigate the effect of Winkler-Pasternak foundations on the static and dynamic behaviors of laminated doble-curved and degenerate shells and panels. Zhang and Liew [29] used an element-free approach for large deflection analysis of functionally graded carbon nanotube reinforced composite (FG-CNTRC) plates on elastic foundations. Ansari et al. [30] applied the differential quadrature method to analyze the effect of elastic ground on the vibrations of the FG-CNTRC spherical shells. Dinh and Nguyen [31] reported the dynamic response and vibration behaviors of truncated conical shells (FG-CNTRC) on elastic foundations using the fourth-order Runge–Kutta method. In the study of Shen and He [32], the large amplitude vibration analysis of FG-CNTRC panels was performed considering the elastic foundation effect and using a two-stage perturbation approach to solve the problem. Babaei et al. [33] examined the large amplitude vibration of functionally graded shallow arches on a non-linear elastic foundation using a two-stage perturbation approach, and the influence of foundations on the frequency parameters is investigated in detail. Sobhy and Zenkour [34] investigated the effect of elastic foundations on the vibration frequency of functionally graded graphene platelet reinforced composite double curved shallow shells in linear formulation. Vu et al. [35] studied the nonlinear dynamics of functionally graded graphene nanoplatelet-reinforced polymer double-curved shallow shells resting on an elastic foundation, using a micromechanical model and applying the Galerkin method. Sofiyev and co-authors [36,37] solved the linear stability problems of carbon nanotube reinforced composite conical shells under hydrostatic pressure and combined loads within shear deformation theory by considering the effect of elastic foundations. Zhang et al. [38] presented nonlinear bending analysis of functionally graded CNT-reinforced shallow arches placed on elastic foundations using a two-step perturbation technique. Despite the difficulties in deriving and solving the basic equations, shear deformation theories give more realistic results when studying the nonlinear static and dynamic behavior of composite structures. This factor has led to the emergence of many theories of shear deformation [39–42].

A review of the literature shows that the nonlinear free vibration frequency-amplitude dependence of double-curved shell structures consisting of nanocomposites resting on elastic soils has not been sufficiently studied analytically in the framework of ST. The main purpose of this study is to examine the change in the effect of transverse shear deformations and heterogeneity on nonlinear frequency values of nanocomposite double-curved shell structures in the presence of elastic soils.

## 2. Theoretical formulation

### 2.1. Basic relations and equations

The double-curved nanocomposite shallow shells such as spherical and hyperbolic paraboloid (hypar) shells with thickness $h$, radii $r_1$ and $r_2$, and length $a$ and $b$ resting on the Pasternak elastic foundation are illustrated in Figs. 1 and 2, respectively. The origin of the coordinate system $(x, y, z)$ is located at the upper left end of the middle surface of the structure.

The following displacement fields are used to model the shear deformation across the shallow shell thickness in the present study [39]:

$$u_1(x,y,z) = u(x,y) + z\varphi_1(x,y),\ \ v_1(x,y,z) = v(x,y) + z\varphi_2(x,y),\ \ w_1(x,y,z) = w(x,y) \tag{1}$$

where the displacements in the mid-surface corresponding to the directions of the coordinate axes are denoted by $u, v, w$, respectively, $\varphi_1$ and $\varphi_2$ are rotations of normal to the mid-surface of the shallow shell with respect to the $y$ and $x$ axes, respectively.

The reaction-deflection relationship of the two-parameter elastic foundation is defined by Pasternak as follows [25,26]:

$$K(w) = k_w w - k_p\left(w_{,xx} + w_{,yy}\right) \tag{2}$$

where $k_w$ (in N/m$^3$) is the spring stiffness and $k_P$ (in N/m) is shearing layer stiffness as $k_P = 0$, the two-parameter elastic foundation becomes a one-parameter or Winkler elastic foundation (WEF). Here the comma denotes partial derivative with respect to the coordinates.

The specification of the mechanical properties of the nanocomposite shells as a function of the thickness coordinate is based on the extended mixing rule and is expressed as [13]:

$$Y_{\bar{z}}^{(11)} = \eta^{(1)} V_{\bar{z}}^{(cnt)} Y_{11}^{(cnt)} + V^{(m)} E^{(m)},\ \ Y_{\bar{z}}^{(22)} = \eta^{(2)}\left[\frac{V_{\bar{z}}^{(cnt)}}{Y_{22}^{(cnt)}} + \frac{V^{(m)}}{E^{(m)}}\right]^{-1},$$

$$Y_{\bar{z}}^{(12)} = \eta^{(3)}\left[\frac{V_{\bar{z}}^{(cnt)}}{Y_{12}^{(cnt)}} + \frac{V^{(m)}}{Y^{(m)}}\right]^{-1},\ \ Y_{\bar{z}}^{(13)} = Y_{\bar{z}}^{(12)},\ \ Y_{\bar{z}}^{(23)} = 1.2Y_{\bar{z}}^{(12)}, \nu^{(12)} = V_*^{(cnt)}\nu_{12}^{(cnt)} + V^{(m)}\nu^{(m)}, \tag{3}$$

$$\nu^{(12)}Y_{\bar{z}}^{(22)} = \nu^{(21)}Y_{\bar{z}}^{(11)}, \rho^{(mix)} = V_*^{(cnt)}\rho^{(cnt)} + V^{(m)}\rho^{(m)}, \bar{z} = z/h$$

where the Young and shear moduli for CNTs and matrix are denoted by $Y_{ij}^{(cnt)}(i,j = 1,2)$, and $Y^{(m)}$, $G^{(m)}$ , respectively, the corresponding densities are denoted by $\rho^{(cnt)}$ and $\rho^{(m)}$, and efficiency parameters of

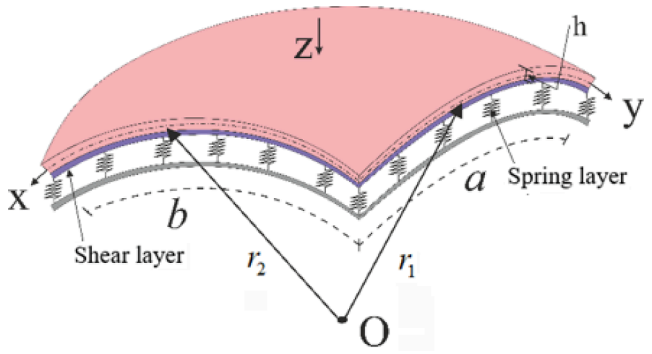


**Fig. 1.** Nanocomposite spherical shell on the Pasternak elastic foundation and coordinate system.

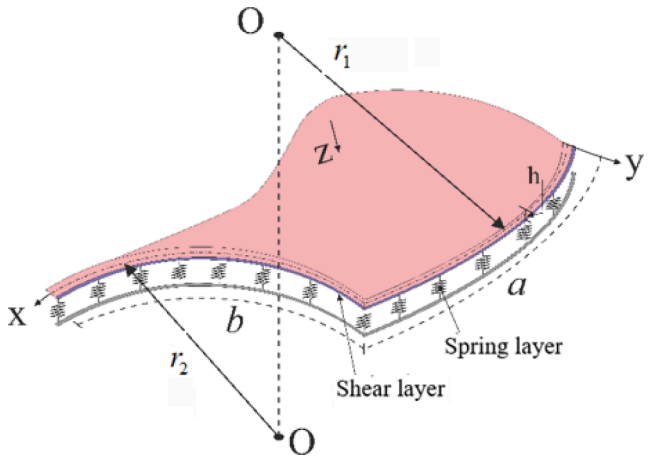


**Fig. 2.** Nanocomposite hypar shell on the Pasternak elastic foundation and coordinate system.

CNTs are denoted by $\eta^{(i)}(i = 1, 2, 3)$. Here $V_{\bar{z}}^{(cnt)}$ and $V^{(m)}$ denote the volume fraction of CNTs and matrix that obey the rule of $V_{\bar{z}}^{(cnt)} + V^{(m)} = 1$. For the total volume fraction of CNTs are used the following relation:

$$V_*^{(cnt)} = \frac{w^{(cnt)}}{w^{(cnt)} + (\rho^{(cnt)}/\rho^{(m)})(1 - w^{(cnt)})} \tag{4}$$

where $w^{(cnt)}$ denotes the mass of CNTs.

It is assumed that the volume fractions change uniformly and with three different linear functions depending on the thickness coordinate, modeled as follows (see, Fig. 3):

$$V_{\bar{z}}^{(cnt)} = \begin{cases} US \ \text{ when } \ V_*^{(cnt)} \\ VS \ \text{ when } \ \left(1 - \frac{Z}{h}\right) V_*^{(cnt)} \\ OS \ \text{ when } \ \left(1 + \frac{Z}{h}\right) V_*^{(cnt)} \\ XS \ \text{ when } \ 4\left|\frac{Z}{h}\right| V_*^{(cnt)} \end{cases} \tag{5}$$

where US shows a uniform or U-shaped distribution, VS, V-shaped, OS, O-shaped and XS, X-shaped distribution of CNTs in the matrix.

The mathematical model of Hooke's stress–strain law for nanocomposite structural elements based on the ST can be written as [13–16]:

$$\begin{bmatrix} \sigma^{(11)} \\ \sigma^{(22)} \\ \sigma^{(12)} \end{bmatrix} = \begin{bmatrix} Q_{\bar{z}}^{(11)} Q_{\bar{z}}^{(12)} 0 \\ Q_{\bar{z}}^{(21)} Q_{\bar{z}}^{(22)} 0 \\ 00 Q_{\bar{z}}^{(66)} \end{bmatrix} \begin{bmatrix} e^{(11)} \\ e^{(22)} \\ \gamma^{(12)} \end{bmatrix} \tag{6.1}$$

and

$$\begin{bmatrix} \sigma^{(13)} \\ \sigma^{(23)} \end{bmatrix} = \begin{bmatrix} Q_{\bar{z}}^{55} 0 \\ 0 Q_{\bar{z}}^{44} \end{bmatrix} \begin{bmatrix} \gamma^{(13)} \\ \gamma^{(23)} \end{bmatrix} \tag{6.2}$$

where $[\sigma]$ and $[e]$ are stress and strain tensors, and $Q_{\bar{z}}^{(ij)}(i = 1, 2, j = 1, 2, 3)$ are described as:

$$Q_{\bar{z}}^{(11)} = \frac{Y_{\bar{z}}^{(11)}}{1 - \nu^{(12)}\nu^{(21)}}, Q_{\bar{z}}^{(12)} = \frac{\nu^{(21)} Y_{\bar{z}}^{(11)}}{1 - \nu^{(12)}\nu^{(21)}} = \frac{\nu^{(12)} Y_{\bar{z}}^{(22)}}{1 - \nu^{(12)}\nu^{(21)}} = Q_{\bar{z}}^{(21)}, Q_{\bar{z}}^{(22)} = \frac{Y_{\bar{z}}^{(22)}}{1 - \nu^{(12)}\nu^{(21)}}$$

$$Q_{\bar{z}}^{(44)} = G_{\bar{z}}^{(23)}, Q_{\bar{z}}^{(55)} = G_{\bar{z}}^{(13)}, Q_{\bar{z}}^{(66)} = G_{\bar{z}}^{(12)} \tag{7}$$

It is assumed that the transverse shear strains are distributed parabolic ($f_{\bar{z}} = 1 - 4\bar{z}^2$) throughout the shell thickness. It should also be emphasized that using a shear correction factor may not yield reasonable results in structural elements consisting of heterogeneous or functionally graded materials. Because the shear correction factor is reasonable for structural elements consisting of homogeneous composite materials. One of the advantages of this theory is that a shear correction factor is not required. Let the force components be defined as $T_{11} = h\Phi_{,yy}$, $T_{22} = h\Phi_{,xx}$, $T_{12} = -h\Phi_{,xy}$, where $\Phi$ is the stress function.

In this study, considering geometric nonlinearity based on the von Karman-Donnell assumptions based on the ST, the kinematic relationship between strains with displacements and angles of rotation for nanocomposite structural elements with double curvature is built as follows [39–45]:

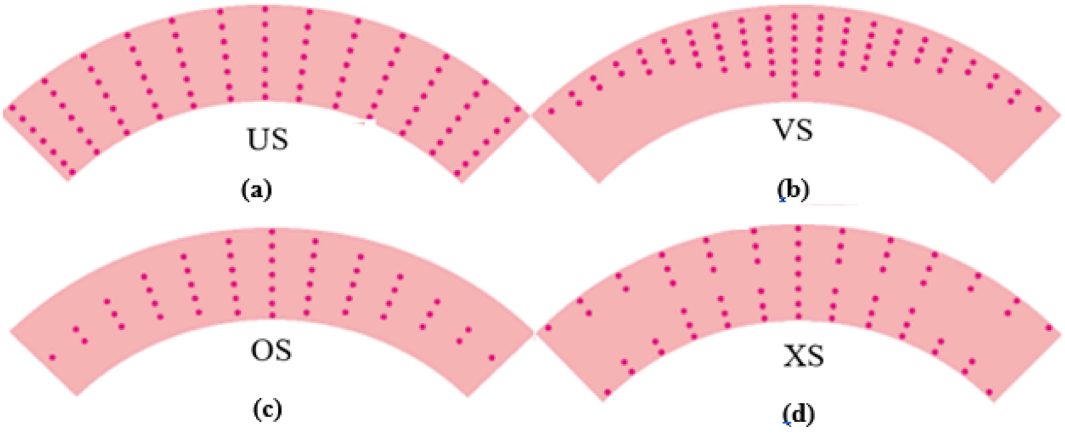


**Fig. 3.** Volumetric distribution (a) uniform (US) and with three different linear functions (b) V-shaped (abbreviated as VS), (c) O-shaped (OS) and (d) X-shaped (XS).

$$e^{11} = e_0^{11} - zw_{,xx} + \theta_{1z}\varphi_{1,x}, e^{22} = e_0^{22} - zw_{,yy} + \theta_{2z}\varphi_{2,y}, \gamma^{12} = \gamma_0^{12} - 2zw_{,xy} + \theta_{1z}\varphi_{1,y} + \theta_{2z}\varphi_{2,x} \quad (9)$$

where

$$e_0^{(11)} = u_{,x} - w/r_1 + 0.5\left(w_{,x}\right)^2, e_0^{(22)} = v_{,x} - w/r_2 + 0.5\left(w_{,y}\right)^2, \gamma_0^{(12)} = w_{,x} + w_{,y} + w_{,x}w_{,y}$$

$$\theta_{1z} = h\int_0^{\bar{z}} \frac{1-4\bar{z}^2}{G_{\bar{z}}^{13}} d\bar{z}, \theta_{2z} = h\int_0^{\bar{z}} \frac{1-4\bar{z}^2}{G_{\bar{z}}^{23}} d\bar{z} \quad (10)$$

The integration of the stresses through the section yields the forces $\left(T_{ij},\ N_j\right)$ and moments $M_{ij}$ [39–45]:

$$\left(T_{ij}, N_j\right) = h\int_{-1/2}^{1/2} \left(\sigma^{(ij)}, \sigma^{(1j_1)}\right) d\bar{z}, M_{ij} = h^2 \int_{-1/2}^{1/2} \sigma^{(ij)}\bar{z}d\bar{z} (i,j = 1,2,j_1 = 2,3) \quad (11)$$

Considering the nonlinearity and using highlighted ST, the equations of compatibility and motion for nanocomposite shallow shells with double curvature resting on Pasternak elastic foundation can be obtained in terms of the stress function Φ, two rotation functions $\varphi_1$ and $\varphi_2$, and deflection function $w$ as follows:

$$\begin{aligned} &h\left[b_{11}\Phi_{,yyyy} + (b_{12} + b_{21} + b_{31})\Phi_{,xxyy} + b_{22}\Phi_{,xxxx}\right] - b_{23}w_{,xxxx} - (b_{24} + b_{13} - b_{32})w_{,xxyy} \\ &-b_{14}w_{,yyyy} + \left(w_{,xx}/r_2 + w_{,yy}/r_1\right) - \left(w_{,xy}\right)^2 + \mathrm{w_{,xx}w_{,yy}} + \mathrm{b_{25}}\varphi_{1,xxx} + (\mathrm{b_{15}} + \mathrm{b_{35}})\varphi_{1,xyy} \\ &+(b_{28} + b_{38})\varphi_{2,xxy} + b_{18}\varphi_1\varphi_{1,yyy} = 0 \end{aligned} \quad (12)$$

## 3. Solution of problem

The deflection and rotation angle functions for nanocomposite shallow shells in which all edges satisfy the simply supported boundary conditions are sought as follows [39,46]:

$$w = \overline{w}(t)\sin(\mathrm{m_1 x})\sin(\mathrm{n_1 y}),\ \varphi_1 = \overline{\varphi}_1(t)\cos(\mathrm{m_1 x})\sin(\mathrm{n_1 y}),\ \varphi_2 = \overline{\varphi}_2(t)\sin(\mathrm{m_1 x})\cos(\mathrm{n_1 y}) \quad (14)$$

where $\overline{w}(t)$ and $\overline{\varphi}_k(t)$ (k= 1, 2) are time-dependent functions, $m_1 = \mathrm{m}\pi/\mathrm{a}$, $\mathrm{n_1} = \mathrm{n}\pi/\mathrm{b}$, in which $(m, n)$ is vibrational mode in directions of $x$ and $y$, respectively.

Incorporating (14) into Eq. (12), we obtain the expression of the Airy stress function with time- dependent deflection and rotation angle functions from a particular solution of the nonhomogeneous differential equation:

$$\Phi = \chi_1\overline{w}^2(t)cos(2m_1x) + \chi_2\overline{w}^2(t)cos(2n_1y) + [\chi_{31}\overline{w}(t) + \chi_{32}\overline{\varphi}_1(t) + \chi_{33}\overline{\varphi}_2(t)]sin(m_1x)sin(n_1y) \quad (15)$$

where:

$$\chi_1 = \frac{\mathrm{n_1^2}}{32\mathrm{m_1^2 b_{22} h}},\ \chi_2 = \frac{\mathrm{m_1^2}}{32\mathrm{n_1^2 b_{11} h}},\ \chi_{31} = \frac{\mathrm{b_{23}m_1^4} + (\mathrm{b_{24}} + \mathrm{b_{13}} - \mathrm{b_{32}})\mathrm{m_1^2 n_1^2} + \mathrm{b_{14}n_1^4} + \frac{\mathrm{m_1^2}}{\mathrm{r_2}} + \frac{\mathrm{n_1^2}}{\mathrm{r_1}}}{\mathrm{h[b_{11}n_1^4 + (b_{12} + b_{21} + b_{31})m_1^2 n_1^2 + b_{22}m_1^4]}},$$
$$\chi_{32} = \frac{-\mathrm{b_{25}m_1^3} - (\mathrm{b_{15}} + \mathrm{b_{35}})\mathrm{m_1 n_1^2}}{\mathrm{h[b_{11}n_1^4 + (b_{12} + b_{21} + b_{31})m_1^2 n_1^2 + b_{22}m_1^4]}}, \chi_{33} = \frac{-(\mathrm{b_{28}} + \mathrm{b_{38}})\mathrm{m_1^2 n_1} - \mathrm{b_{18}n_1^3}}{\mathrm{h[b_{11}n_1^4 + (b_{12} + b_{21} + b_{31})m_1^2 n_1^2 + b_{22}m_1^4]}} \quad (16)$$

and

$$\begin{aligned} &h\left[(\mathrm{c_{11}} - \mathrm{c_{31}})\Phi_{,xxyy} + \mathrm{c_{12}}\Phi_{,xxxx}\right] + \rho^{(1)}\ddot{w}_{,xx} - c_{13}w_{,xxxx} - (c_{14} + c_{32})w_{,xxyy} \\ &+ c_{15}\varphi_{1,xxx} + c_{35}\varphi_{1,xyy} - \theta_3\varphi_{1,x} - \rho^{(2)}\ddot{\varphi}_{1,x} + (c_{18} + c_{38})\varphi_{2,xxy} \\ &= 0,\ hc_{21}\Phi_{,yyyy} + h(c_{22} - c_{31})\Phi_{,xxyy} - (c_{32} + c_{23})w_{,xxyy} - c_{24}w_{,yyyy} \\ &+ \rho^{(1)}\ddot{w}_{,xx} + (c_{35} + c_{25})\varphi_{1,xyy} + c_{38}\varphi_{2,xxy} + c_{28}\varphi_{2,yyy} - \theta_4\varphi_{2,y} - \rho^{(3)}\ddot{\varphi}_{2,y} \\ &= 0,\ h\left(\Phi_{,xx}/r_2 + \Phi_{,yy}/r_1\right) - \rho^{(mix)}h\ddot{w} + \theta_3\varphi_{1,x} + \theta_4\varphi_{2,y} + h\left(\Phi_{,yy}w_{,xx} - 2\Phi_{,xy}\mathrm{w_{,xy}} + \Phi_{,xx}\mathrm{w_{,yy}}\right) + k_w w - k_p\left(w_{,xx} + w_{,yy}\right) \\ &= 0. \end{aligned} \quad (13)$$

where "··" denotes the second-order derivative with respect to the time, and the coefficients $b_{ij}$, $c_{ij}, \rho^{(i)} (i = 1,2,3, j = 1,2,\ldots,8)$ and $\theta_j (j = 3,4)$ are described in the Appendix A.

By substituting the expression (14) and (15) into the system of partial differential Eq. (13) and applying the Galerkin method in the integration domain $\Pi = \{(x,y),\ 0 \leqslant x \leqslant a,\ 0 \leqslant y \leqslant b\}$, then ignoring the inertial terms denoted by the superscript $t$ from the system of equations that arise due to their small effects, and eliminating the rotation functions $\overline{\varphi}_1(t)$ and $\overline{\varphi}_2(t)$ from these three equations, we get the following ordinary differential equation with second- and third-order nonlinear terms:

$$\ddot{\overline{w}} + \left(\Omega_{ST}^{wpL}\right)^2 F(t) = 0 \quad (17)$$

where $\left(\Omega_{ST}^{lwp}\right)^2$ is the square of linear frequency (*LF*) for nanocomposite shells with double curvature on Pasternak-type elastic foundation in the scope of ST, $F(t)$ will determine the elastic characteristic of the shell-foundation system over the entire range of considered amplitudes and the following definitions apply:

$$\left(\Omega_{ST}^{wpL}\right)^2 = \frac{\overline{p}_{31} + k_w + k_p(m_1^2 + n_1^2)}{\rho^{(mix)}h} \quad (18)$$

$$F(t)=\left[1+\frac{q_1}{\left(\Omega_{ST}^{wpL}\right)^2}\overline{w}(t)+\frac{q_2}{\left(\Omega_{ST}^{wpL}\right)^2}\overline{w}^2(t)\right]\overline{w}(t) \tag{19}$$

in which

$$q_1=\frac{\overline{p}_{31}^{NL}}{\rho^{(mix)}h},\ q_2=\frac{p_{32}}{\rho^{(mix)}h},\ \overline{p}_{31}=p_{31}-\frac{p_{21}p_{34}}{p_{23}}+\frac{p_{11}p_{23}-p_{21}p_{13}}{p_{22}p_{13}-p_{23}p_{12}}\left(p_{33}-\frac{p_{22}p_{34}}{p_{23}}\right)$$
$$\overline{p}_{31}^{NL}=p_{31}^{NL}-\frac{p_{34}p_{21}^{NL}}{p_{23}}+\frac{p_{11}^{NL}p_{23}-p_{13}p_{21}^{NL}}{p_{12}p_{23}-p_{13}p_{22}}\left(\frac{p_{34}p_{22}}{p_{23}}-p_{33}\right) \tag{20}$$

Here $p_{ij}(i=1,2,3,j=1,2,...,4)$ are described in Appendix B.

The trial function with initial conditions $\overline{w}=\overline{w}_0,\ \dot{\overline{w}}=0$ when $t=0$ is sought as follows:

$$\overline{w}(t)=Acos\left(\Omega_{wpST}^{NL}t\right) \tag{21}$$

where $A$ is the maximum amplitude of the displacement $w$.

To determine the nonlinear frequency ($NF$)-amplitude dependence for nanocomposite structural elements with double curvature resting on elastic foundations, the left side of Eq. (17) is multiplied by the weight function $cos\left(\Omega_{wpST}^{NL}t\right)$ and integrates from 0 to $\pi/(2\Omega_{wpST}^{NL})$ according to parameter $t$ [47]:

$$\int_0^{\frac{\pi}{2\Omega_{wpST}^{NL}}}\left[\ddot{\overline{w}}+\left(\Omega_{ST}^{wpL}\right)^2F(t)\right]cos\left(\Omega_{wpST}^{NL}t\right)\mathrm{d}t=0 \tag{22}$$

where $\Omega_{wpST}^{NL}$ is the $NF$ for nanocomposite shells with double curvature on elastic foundations in the framework of ST.

Substituting (21) into (22) and considering $q_{11}=q_1h$ and $q_{2q}=q_2h^2$, after integrating, we obtain the $NF$-amplitude dependence for nanocomposite structural elements with double curvature resting on elastic foundations as:

$$\Omega_{wpST}^{NL}=\left[\left(\Omega_{ST}^{wpL}\right)^2+\frac{8q_{11}}{3\pi}\frac{A}{h}+\frac{3q_{12}}{4}\left(\frac{A}{h}\right)^2\right]^{1/2} \tag{23}$$

The $NF/LF$ ratio of nanocomposite shells with double curvature sitting on the soils is found from the following equation:

$$\varpi_{wpST}^{NL/L}=\left[\frac{\Omega_{ST}^{wpL}}{\Omega_{ST}^{L}}+\frac{8q_{11}}{3\pi\left(\Omega_{ST}^{L}\right)^2}\frac{A}{h}+\frac{3q_{12}}{4\left(\Omega_{ST}^{L}\right)^2}\left(\frac{A}{h}\right)^2\right]^{1/2} \tag{24}$$

where the following definition is applied: $\varpi_{wpsdt}^{NL/L}=\frac{\Omega_{wpST}^{NL}}{\Omega_{ST}^{L}}$.

In order to obtain $LF$ and $NF$-amplitude relations and the $NF/LF$ ratio of the highlighted frequencies in the framework of the CT, the transverse shear deformations are ignored from the fundamental relations.

When $k_p=0$, the formulas (18), (23) and (24) can be used to find $LF$, $NF$ and $NF/LF$ of doubly-curved shells on the Winkler ground.

When $r_2=-r_1$, the highlighted expressions can be used to find the frequencies and their ratio for hypar shells.

## 4. Numerical analyzes

The purpose of this section is to confirm the accuracy of the analytical solution and to numerically demonstrate the practical importance and originality of the study with application examples. The magnitudes of dimensionless frequency parameter $\Omega_{1ST}^{L}=\Omega_{ST}^{L}\frac{a^2}{h}\left[\frac{\rho^{(m)}}{E^{(m)}}\right]^{0.5}$ for nanocomposite spherical shells reinforced with CNTs without elastic ground are compared with the results of Pouresmaeeli and Fazelzadeh [14]. The data considered in the comparison are: $(m,\ n)=(1,1)$, $h=0.05a$, $b/a=1$, $2a=r_1$ (Table 1). The expression (18) is used to compare with the linear frequency values in the study [14]. Poly methyl methacrylate (PMMA) is used as the main element and CNTs are used as additives. The characteristics of the components that make up the nanocomposite structures are as follows, respectively: $Y^{(m)}=2.1\,\mathrm{GPa}$, $\nu^{(m)}=0.34$, $\rho^{(m)}=1150\,\mathrm{kg/m^3}$ and $Y_{11}^{(cnt)}=5.6466\,\mathrm{TPa}$, $Y_{22}^{(cnt)}=7.08\,\mathrm{TPa}$, $Y_{12}^{(cnt)}=1.9445\,\mathrm{TPa}$, $\nu_{12}^{(cnt)}=0.175$, $\rho^{(cnt)}=1400\,\mathrm{kg/m^3}$. The efficiency parameters of CNTs are used as in Ref [14]: $\eta^{(1)}=0.149$, $\eta^{(2)}=\eta^{(3)}=0.934$ for $V_*^{(cnt)}=0.11$, $\eta^{(1)}=0.15$, $\eta^{(2)}=\eta^{(3)}=0.941$ for $V_*^{(cnt)}=0.14$ and $\eta^{(1)}=0.149$, $\eta^{(2)}=\eta^{(3)}=1.381$ for $V_*^{(cnt)}=0.17$. When the dimensionless linear frequency magnitudes of CNT reinforced spherical shells are compared in both studies, it is seen that the maximum difference is 0.945% in the VS distribution, and the least difference is 0.036% in the XS distribution. As can be seen, the difference between both studies is reasonable.

The target stage after comparison is to examine in detail the effects of soils on the $NF$ -amplitude dependence for homogeneous and inhomogeneous nanocomposite spherical and hypar shells, by performing original numerical analysis. Here, unique numerical analyzes and interpretations of nonlinear frequency amplitude dependence with and without the elastic foundation are presented using different CNT patterns and volume fractions and geometrical properties within the framework of CT and ST. Numerical analyzes were performed using expressions (23) and (24), and the abbreviations for classical theory and shear deformation theory will be denoted as CT and ST, respectively. The vibration mode is considered as (m, n) = (1,1). The negative sign in percentages indicates that inhomogeneous frequency values are smaller than those in a uniform distribution. The following expressions are used for the percentages of the influences of elastic soils, material gradient and transverse shear deformations (TSDs) on the $NF$: $\frac{\Omega_{HTP}-\Omega_{UP}}{\Omega_{UP}}\times 100\%$, $\frac{\Omega_{CT}^{NL}-\Omega_{ST}^{NL}}{\Omega_{CT}^{NL}}\times 100\%$, $\frac{\Omega_{wpST}^{NL}-\Omega_{ST}^{NL}}{\Omega_{ST}^{NL}}\times 100\%$, $\frac{\varpi_{wpST}^{NL/L}-\varpi_{ST}^{NL/L}}{\varpi_{ST}^{NL/L}}\times 100\%$. The properties of the components of nanocomposite shells made of PMMA and CNT are as follows: $Y^{(m)}=2.5\,\mathrm{GPa}$, $\nu^{(\mathrm{m})}=0.34$, $\rho^{(\mathrm{m})}=1150\,\mathrm{kg/m^3}$ and $Y_{11}^{(cnt)}=5.6466\,\mathrm{TPa}$, $Y_{22}^{(cnt)}=7.08\,\mathrm{TPa}$, $Y_{12}^{(cnt)}=1.9445\,\mathrm{TPa}$, $\nu_{12}^{(\mathrm{cnt})}=0.175$, $\rho^{(cnt)}=1400\ \mathrm{kg/m^3}$, respectively, the total volume fractions and efficiency parameters of carbon nanotubes are used as in Shen [13]): $\eta^{(1)}=0.137$, $\eta^{(2)}=1.022,\eta^{(3)}=0.715$ for $V_*^{(cnt)}=0.12$, $\eta^{(1)}=0.142$, $\eta^{(2)}=1.626$, $\eta^{(3)}=1.138$ for $V_*^{(cnt)}=0.17$ and $\eta^{(1)}=0.141$, $\eta^{(2)}=1.585$, $\eta^{(3)}=1.109$ for $V_*^{(cnt)}=0.28$.

**Table 1**
The comparison $\Omega_{1sdt}^{L}$ for nanocomposite spherical shells reinforced with CNTs without elastic foundation.

| $V_{cn}^{*(1)}$ | $\Omega_{1ST}^{L}=\Omega_{ST}^{L}\frac{a^2}{h}\left[\frac{\rho^{(m)}}{E^{(m)}}\right]^{0.5}$ | | | | | | | | |
|---|---|---|---|---|---|---|---|---|---|
| | US | | | VS | | | XS | | |
| | Ref. [14] | Present study | Difference % | Ref. [14] | Present study | Difference % | Ref. [14] | Present study | Difference % |
| 0.11 | 20.238 | 20.286 | 0.237 | 18.543 | 18.685 | 0.766 | 22.432 | 22.493 | 0.272 |
| 0.14 | 21.655 | 21.756 | 0.466 | 19.779 | 19.966 | 0.945 | 23.997 | 24.064 | 0.279 |
| 0.17 | 25.021 | 25.158 | 0.548 | 22.951 | 23.165 | 0.932 | 27.883 | 27.893 | 0.036 |

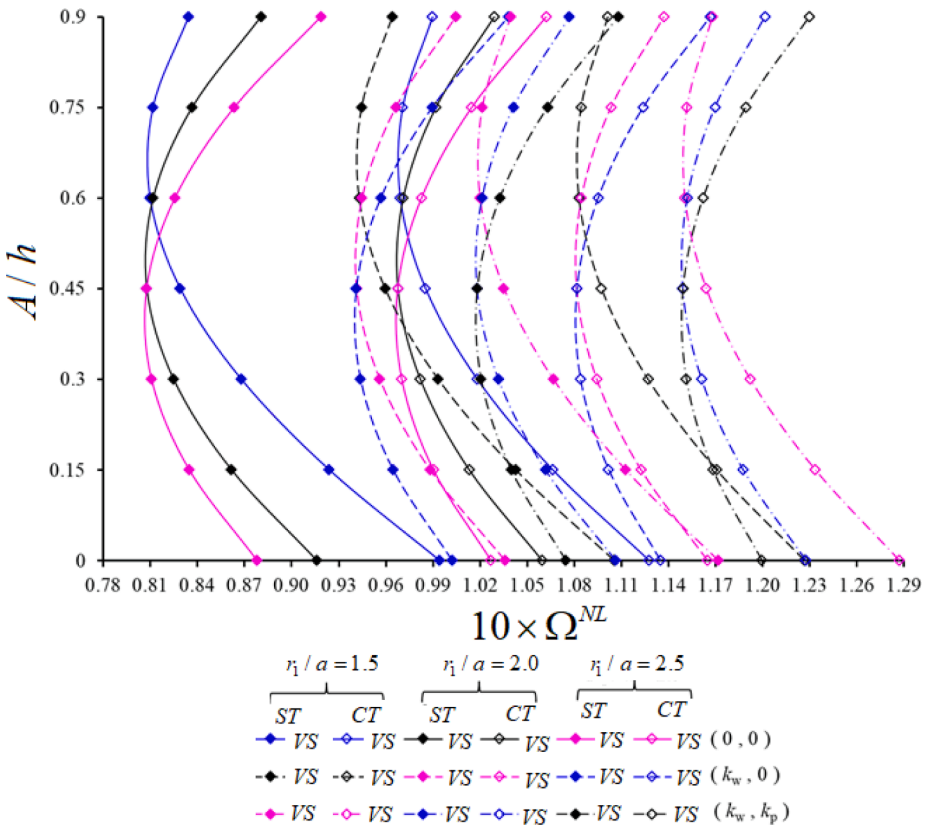


**Fig. 4.** Distribution of the *NF* for spherical shells consisting of V-shaped nanocomposites on various soils depending on the $A/h$ ratio for different $r_1/a$.

**Table 2**
Variation of the *NF* for spherical shells made of O-shaped nanocomposites on and off soils with respect to $A/h$ for different $V_*^{(cnt)}$.

| $\varpi^{NL/L}$ | | $k_w = k_p = 0$ | | $k_w = 2.6 \times 10^9$, $k_p = 0$ | | $k_w = 2.6 \times 10^9, k_p = 15.2 \times 10^4$ | |
|---|---|---|---|---|---|---|---|
| $V_*^{(cnt)}$ | $A/h$ | *ST* | *CT* | *ST* | *CT* | *ST* | *CT* |
| 0.12 | 0 | 1.000 | 1.000 | 1.024 | 1.018 | 1.181 | 1.139 |
| | 0.15 | 0.943 | 0.957 | 0.968 | 0.976 | 1.133 | 1.102 |
| | 0.3 | 0.897 | 0.923 | 0.924 | 0.942 | 1.095 | 1.072 |
| | 0.45 | 0.865 | 0.899 | 0.892 | 0.919 | 1.069 | 1.051 |
| | 0.6 | 0.847 | 0.885 | 0.875 | 0.906 | 1.055 | 1.040 |
| | 0.75 | 0.845 | 0.884 | 0.873 | 0.904 | 1.053 | 1.039 |
| | 0.9 | 0.859 | 0.893 | 0.887 | 0.913 | 1.065 | 1.047 |
| 0.17 | 0 | 1.000 | 1.000 | 1.014 | 1.011 | 1.112 | 1.088 |
| | 0.15 | 0.947 | 0.958 | 0.962 | 0.970 | 1.064 | 1.050 |
| | 0.3 | 0.904 | 0.925 | 0.920 | 0.937 | 1.026 | 1.020 |
| | 0.45 | 0.874 | 0.901 | 0.890 | 0.914 | 1.000 | 0.999 |
| | 0.6 | 0.857 | 0.888 | 0.873 | 0.901 | 0.985 | 0.987 |
| | 0.75 | 0.854 | 0.886 | 0.871 | 0.898 | 0.983 | 0.985 |
| | 0.9 | 0.866 | 0.894 | 0.882 | 0.907 | 0.993 | 0.992 |
| 0.28 | 0 | 1.000 | 1.000 | 1.012 | 1.008 | 1.092 | 1.067 |
| | 0.15 | 0.937 | 0.955 | 0.950 | 0.964 | 1.035 | 1.025 |
| | 0.3 | 0.887 | 0.919 | 0.900 | 0.928 | 0.990 | 0.992 |
| | 0.45 | 0.851 | 0.894 | 0.865 | 0.903 | 0.958 | 0.969 |
| | 0.6 | 0.832 | 0.880 | 0.846 | 0.890 | 0.940 | 0.956 |
| | 0.75 | 0.830 | 0.878 | 0.844 | 0.888 | 0.938 | 0.954 |
| | 0.9 | 0.845 | 0.888 | 0.859 | 0.898 | 0.952 | 0.964 |

The distribution of the *NF* for the spherical shells consisting of V-shaped (or VS) nanocomposites on various soils for different $r_1/a$ ratios, depending on the $A/h$ ratio is drawn in Fig. 4. The data used in numerical calculations are: $a/h = 15$, $V_*^{(cnt)} = 0.28$, $a/b = 0.5, (k_w, 0) = (3.1 \times 10^9, 0), (k_w, k_p) = (3.1 \times 10^9, 1.45 \times 10^5)$. When the $A/h$ ratio increases up to 0.75, the values of *NF* for spherical shells consisting of V-shaped nanocomposites without ground decrease within ST and CT, and then increase after taking the minimum value. In V-shaped spherical shells resting on Winkler and Pasternak soils, *NF* values achieve their minimum value before when$A/h = 0.6$. In the fixed values of the $r_1/a$ ratio, the effect of TSDs on *NF* values for V-shaped nanocomposite spheres on and off the ground, first increases with the increase of $A/h$, and decreases after the frequency takes a minimum value. It is observed that the effect of TSDs on frequency shows a weak decrease when $r_1/a$ increment. Considering the ground effect significantly reduces TSDs effect. For example, at$A/h = 0.6$ and$r_1/a = 1.5$, the effect of TSDs on the *NF* for the unconstrained V-shaped spherical shell is 16.46%, it is 12.93% and 11.36% when the shell resting on Winkler and Pasternak grounds, respectively. Although the foundations effect significantly increases *NF* values, it should be emphasized that the Pasternak ground effect is greater than the Winkler ground effect on the *NF* values. In addition, it is seen that the ground effect on *NF* values is more pronounced in the framework of ST. For the considered data, the largest effect of Winkler foundation on *NF* values in the ST framework is 16.56%, while the greatest effect of Pasternak foundation reaches 26.9%.

Table 2 shows the variation of the *NF* of spherical shells made of O-shaped (or OS) nanocomposites with and without Winkler and Pasternak

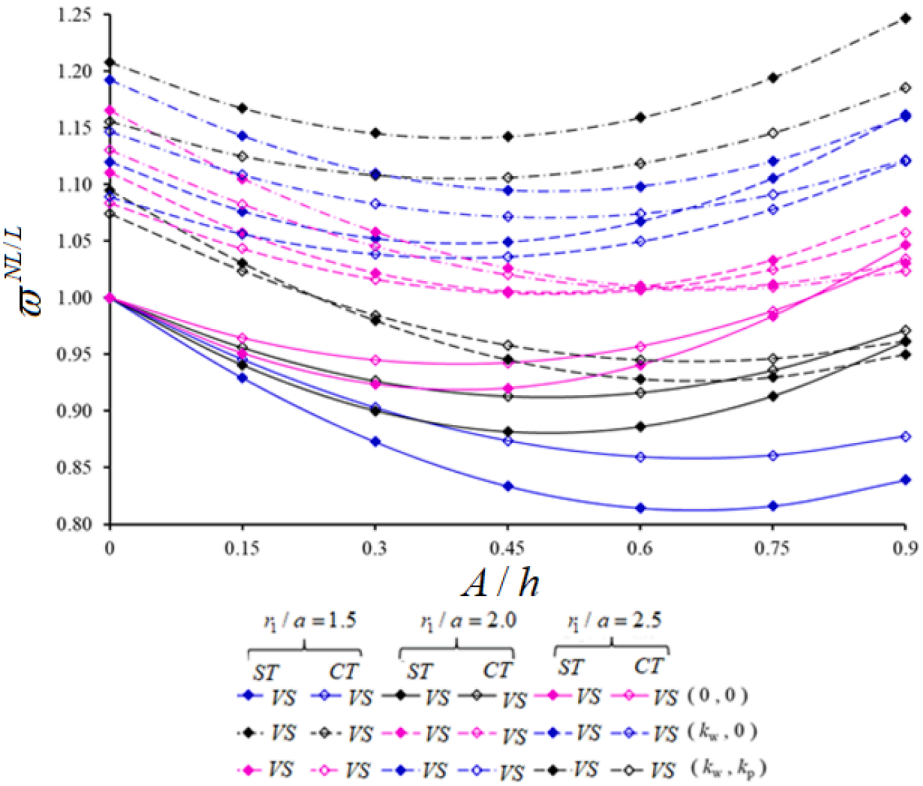


**Fig. 5.** Variation of the *NF*/*LF* ratio for spherical shells composed of V-shaped nanocomposites on various soils ratios according to $A/h$ for different $r_1/a$ and within two shell theories.

soils with respect to the $A/h$ ratio for different $V_*^{(cnt)}$ (=0.12, 0.17 and 0.28). The geometric and ground data in numerical calculations are:$r_1/a = 1,\ a/b = 2,\ a/h = 10, (k_w, 0) = (2.6 \times 10^9,\ 0), (k_w, k_p) = (2.6 \times 10^9, 1.52 \times 10^5)$. When the $V_*^{(cnt)}$ pass from 0.12 to 0.17, the *NF* values of O-shaped spherical shells with and without ground increase weakly, and when the *NF* values pass to 0.28, those become the lowest within the framework of both shell theories. While the spherical shell made of O-shaped nanocomposites, originating from $V_*^{(cnt)} = 0.28$ with and without the foundations, the effect of TSDs is most evident on the *NF* values, while the lowest effects of TSDs in the presence of Winkler and Pasternak soils are observed in O-shaped spherical shells originating from $V_*^{(cnt)} = 0.17$ and $V_*^{(cnt)} = 0.12$, respectively. When the two-parameter elastic soil effect is considered, although the *NF* values increased within both shell theories, the effect of TSDs on NLF values for all volume fractions is significantly reduced, and the most sensitive response to this context is observed at $V_*^{(cnt)} = 0.12$. For example, while$A/h = 0.75$ and$V_*^{(cnt)} = 0.12$, the effects of TSDs on *NF* values are 4.33%, 3.39% and (-1.41%) for baseless, Winkler-based, and Pasternak-based spherical shells, respectively. In addition, the increase of the $A/h$ supported that the TSDs effect remained significant up to the minimum values of the *NF* of spherical shells in the presence and absence of ground for all $V_*^{(cnt)}$.

In Fig. 5, the variation of the *NF*/*LF* ratio for spherical shells composed of V-shaped nanocomposites on various soils with different $r_1/a$ ratios according to $A/h$ is depicted within the framework of two shell theories. The following data were used in numerical calculations: $V_{*(cnt)} = 0.28,\ a/b = 0.5, a/h = 15,\ (k_w, 0) = (2.6 \times 10^9,\ 0),\ (k_w, k_p) = (2.6 \times 10^9, 1.52 \times 10^5)$. For both shell theories, when the $A/h$ ratio increases up to 0.6, the *NF*/*LF* ratio of V-shaped spherical shells without ground decreases parabolically and then increases after taking its minimum value. At fixed values of the $r_1/a$ ratio, the *NF*/*LF* ratio for V-shaped spherical shells on Winkler and Pasternak soils reaches its minimum value before, that is, at$A/h = 0.45$. Although the TSDs effect on the *NF*/*LF* ratio for the spherical shells without ground is significant, it weakens considerably when the ground effect is taken into account. For example, for$A/h = 0.45$ and$r_1/a = 2.5$, the TSDs effect on the *NF*/*LF* ratio is (2.37%) when the V-shaped spherical shells is not on the ground, while the TSDs effects on the *NF*/*LF* ratio in the presence of Winkler and Pasternak soils are (-1.25%) and (−3.30%), respectively. Also, the Pasternak ground effect on the *NF*/*LF* ratio is more pronounced than the Winkler ground effect. In addition, it is seen that from Fig. 5 the ground effect on the *NF*/*LF* F ratio in the framework of ST is more pronounced than the effect in the framework of CT.

The variation of *NF* for spherical and hypar shells consisting of U and V-shaped nanocomposites on and off soils depending on the $A/h$ ratio are presented in Table 3 in the framework of ST and CT. The data used in numerical calculations are: $r_1/a = 1.5,\ a/b = 0.5, a/h = 15, (k_w, 0) = (3.1 \times 10^9,\ 0), (k_w, k_p) = (3.1 \times 10^9, 1.45 \times 10^5),\ V_*^{(cnt)} = 0.28$. When the $A/h$ ratio increases, the *NF* values of U and V-shaped hypar shells on and off soils continuously increase under ST and CT, while those for spherical shells show a parabolic action, that is, they first decrease and then increase after reaching the minimum value. It is easily seen from Table 3 that the *NF* for U and V-shaped hypar shells on and off soils are greater than those of spherical shells. The influence of the V model on *NF* is significant in absence soils, weakening this effect when considering the effect of TSDs, while considering the influence of soil, this effect becomes even weaker. Depending on the increase of the $A/h$ ratio, the V-pattern effect on the *NF* for spherical shells with and without soils increases and decreases after the maximum value, while that effect decreases continuously in the same originating hypar shell. For example,

a) When the $A/h$ ratio increases from 0.15 to 0.6, the V-pattern effect on the *NF* for the unconstrained spherical shell increases from (-8.09%)

**Table 3**
Variation of *NF* for spherical and hypar shells consisting of U and V-shaped nanocomposites on and off soils depending on the $A/h$ ratio in the framework of ST and CT.

$10\times\Omega^{NL}$

| | $k_w=k_p=0$ | | | | Hypar | | | |
|---|---|---|---|---|---|---|---|---|
| | Spherical | | | | | | | |
| | *US* | | *VS* | | *US* | | *VS* | |
| $A/h$ | *ST* | *CT* | *ST* | *CT* | *ST* | *CT* | *ST* | *CT* |
| 0 | 1.070 | 1.306 | 0.994 | 1.128 | 0.967 | 1.223 | 0.878 | 1.027 |
| 0.15 | 1.005 | 1.253 | 0.924 | 1.066 | 1.043 | 1.284 | 0.961 | 1.099 |
| 0.3 | 0.954 | 1.212 | 0.868 | 1.018 | 1.129 | 1.355 | 1.054 | 1.181 |
| 0.45 | 0.919 | 1.185 | 0.829 | 0.985 | 1.224 | 1.434 | 1.154 | 1.272 |
| 0.6 | 0.902 | 1.172 | 0.810 | 0.969 | 1.324 | 1.521 | 1.261 | 1.369 |
| 0.75 | 0.903 | 1.173 | 0.811 | 0.971 | 1.430 | 1.614 | 1.371 | 1.471 |
| 0.9 | 0.924 | 1.189 | 0.834 | 0.990 | 1.540 | 1.712 | 1.485 | 1.578 |
| $A/h$ | $k_w=3.1\times10^9, k_p=14.6\times10^4$ | | | | | | | |
| 0 | 1.237 | 1.445 | 1.172 | 1.287 | 1.149 | 1.371 | 1.075 | 1.200 |
| 0.15 | 1.181 | 1.398 | 1.113 | 1.233 | 1.214 | 1.426 | 1.144 | 1.262 |
| 0.3 | 1.138 | 1.362 | 1.067 | 1.192 | 1.289 | 1.490 | 1.223 | 1.334 |
| 0.45 | 1.109 | 1.337 | 1.035 | 1.164 | 1.372 | 1.563 | 1.311 | 1.415 |
| 0.6 | 1.094 | 1.326 | 1.020 | 1.151 | 1.462 | 1.643 | 1.405 | 1.503 |
| 0.75 | 1.096 | 1.327 | 1.021 | 1.152 | 1.559 | 1.729 | 1.505 | 1.597 |
| 0.9 | 1.113 | 1.341 | 1.039 | 1.168 | 1.660 | 1.821 | 1.609 | 1.695 |

to (-10.21%) and then it regresses to (-9.21%) for$A/h=0.9$, while it for the same originating hypar shell decreases from (-7.88%) to (-4.81%).

b) When the $A/h$ ratio increases from 0.15 to 0.6, the effect of the V-pattern on the *NF* values for the spherical shell on the Pasternak floor increases from (-5.79%) to (-6.82%) and then it regresses to (-6.59%) for A/h = 0.9, while the VS pattern effect in the hypar shell decreases continuously from (-5.76%) to (-3.04%).

The V-shaped effect on *NF* for both nanocomposite shells with and without foundation is more pronounced in CT than the effect in the framework of ST. Thus, considering TSDs in the calculations reduces the significance of the influence of the V-pattern on the *NF* values by about 4–6%. When comparing the effect of TSD on NLF values for spherical and hypar shells with the U and V-patterns, there is a significance of about 3% in the US. When the $A/h$ ratio increases, the TSDs effect on the *NF* increases in the spherical shells and decreases after reaching its highest value, while it in the hypar shells is always in a decreasing action. When the Pasternak foundation effect on the *NF* for spherical and hypar shells is compared, it is more effective in spherical shells and the difference becomes wider with the increase of $A/h$.

The change curves of the $NF/LF$ ratio of the spherical and hypar shells consisting of U and X-origin nanocomposites on and off the ground with respect to $A/h$ are plotted in Fig. 6 in the framework of both shell theories. The following data were used in numerical calculations: $r_1/a=3,\ a/b=1, a/h=15, (k_w,0)=(2.6\times10^9,\ 0),\ (k_w,\ k_p)=(2.6\times\ 10^9,\ 1.52\times10^5),\ V_*^{(cnt)}=0.17$. For both shell theories, the $NF/LF$ ratio of U and X-originating spherical shells on and off the ground decreases parabolically when the $A/h$ ratio increases up to 0.45 and increases after taking its minimum value, while that ratio increases continuously in same originating hypar shells, when the $A/h$ ratio increases up to 0.9. In the framework of ST, the $NF/LF$ ratio of X-originating hypar shells on the Pasternak ground increased from 1.254 to 1.549 with the increase of $A/h$ ratio from 0 to 0.9, while that ratio varies around 1.2 in same originating spherical shells. On the frame of ST, the effect of Pasternak ground on the $NF/LF$ ratio of X-originating hypar shells increases from 23.31% to 25.1% when $A/h$ ratio increases from 0 to 0.45 and decreases to 21.91% for$A/h=0.9$, in same originating spherical shells it decreases continuously from 23.9% to 14.57%. In the absence of ground effect, as the $A/h$ ratio changes from 0.15 to 0.9, the XS effect on the $NF/LF$ ratio of spherical shells changes around 1%, while it varies between (-0.76%) and (-5.03%) in same originating hypar shells. When the ground effect is considered, the XS effect varies between (-3%) and (-4%) in spherical shells originating from X, while the said effect varies between 4% and 6.4% in same originating hypar shells, as the A/h ratio changes from 0.15 to 0.9. When the $A/h$ ratio varies between 0.15 and 0.9, the difference between the $NF/LF$ ratios of the U-originating spherical shells obtained within the framework of ST and CT, varies between (-5.70%) and (-6.66%) as considering the ground effect, while it varies between (-6.9%) and (-8.18%) in the same shell originating from *X*. When the $A/h$ ratio varies between 0.15 and 0.9, the difference between $NF/LF$ ratios in X- originating hypar shells obtained within the framework of ST and CT theories ranges from (–7.73%) to (-11.69%), as ground effect is taken into account, whereas it varied between (-9.21%) and (-14.82%) in the same shell originating from *X*.

## 5. Conclusions

The nonlinear free vibration of nanocomposite structures resting on elastic soils within ST is presented. After modeling the mechanical properties of nanocomposite shell structures containing CNTs and elastic soils, the basic relations, and governing equations of double curved shell structures within the ST are established considering the geometric nonlinearity. The frequencies of nonlinear and linear free vibrations and their ratios for inhomogeneous nanocomposite structures on the soils within the ST are obtained using perturbation methods. After checking the methodology of the research, the effects of soils,

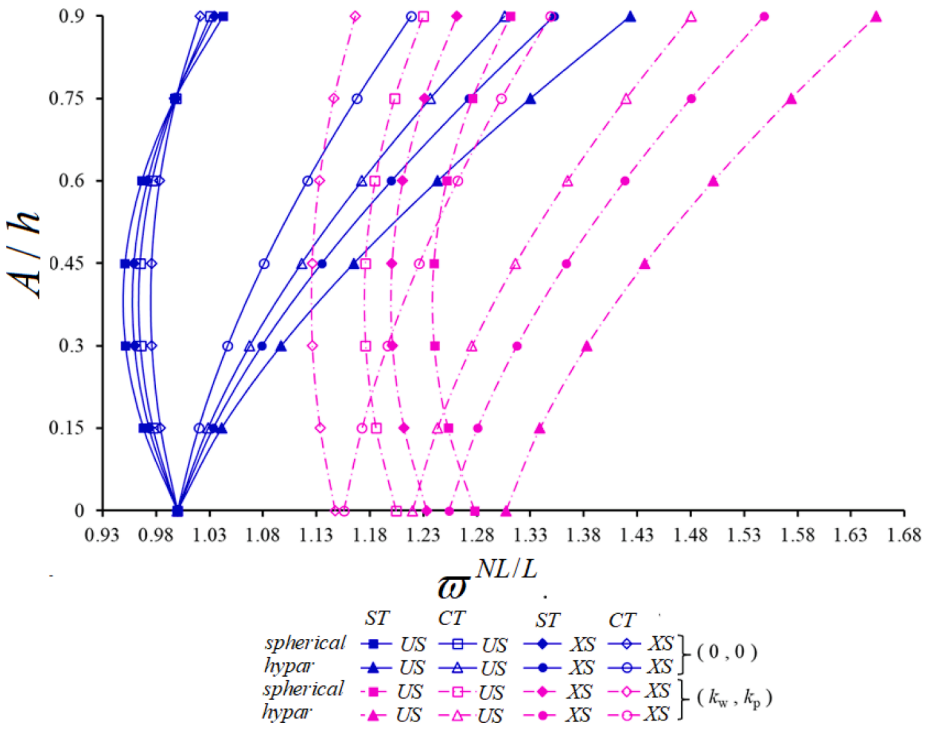


**Fig. 6.** Change of $NF/LF$ ratio of spherical and hypar shells consisting of U and X-origin nanocomposites on and off the ground with respect to $A/h$ in the framework of ST and CT.

nonlinearity, shear strains and patterns of CNT on the frequency-amplitude dependence of nanocomposite structures for various geometric parameters are carried out.

*CRediT authorship contribution statement*

**Avey Mahmure:** Conceptualization, Methodology, Formal analysis, Writing – original draft. **N. Fantuzzi:** Conceptualization, Formal analysis, Writing – review & editing. **A.H. Sofiyev:** Methodology, Formal analysis, Writing – review & editing. **N. Kuruoglu:** Writing – review & editing.

## Declaration of Competing Interest

The authors declare that they have no known competing financial interests or personal relationships that could have appeared to influence the work reported in this paper.

## Appendix A

The coefficients $b_{ij}$, $c_{ij}, \rho^{(i)}$ and $\theta_j$ included in Eqs. (12) and (13) are described as:

$$b_{11}=\frac{a_{220}}{\hbar},\ b_{12}=-\frac{a_{120}}{\hbar},\ b_{13}=\frac{a_{120}a_{211}-a_{111}a_{220}}{\hbar},\ b_{14}=\frac{a_{120}a_{211}-a_{121}a_{220}}{\hbar},$$
$$b_{15}=\frac{a_{250}a_{120}-a_{150}a_{220}}{\hbar}, b_{18}=\frac{a_{280}a_{120}-a_{180}a_{220}}{\hbar},\ b_{21}=-\frac{a_{210}}{\hbar},\ b_{22}=\frac{a_{110}}{\hbar},$$
$$b_{23}=\frac{a_{111}a_{210}-a_{211}a_{110}}{\hbar},\ b_{24}=\frac{a_{121}a_{210}-a_{221}a_{110}}{\hbar},\ b_{25}=\frac{a_{150}a_{210}-a_{250}a_{110}}{\hbar},$$
$$b_{28}=\frac{a_{180}a_{210}-a_{280}a_{110}}{\hbar},\ b_{31}=\frac{1}{a_{660}},\ b_{32}=-\frac{2a_{661}}{a_{660}},\ b_{35}=\frac{a_{350}}{a_{660}},\ b_{38}=\frac{a_{380}}{a_{660}},$$
$$a_{11i_1}=\int_{-h/2}^{h/2}Q_{\bar{z}}^{(11)}z^{i_1}\mathrm{d}z,\ \mathrm{a}_{12i_1}=\int_{-\mathrm{h}/2}^{\mathrm{h}/2}\mathrm{Q}_{\bar{z}}^{(12)}\mathrm{z}^{\mathrm{i}_1}\mathrm{d}z,\ \mathrm{a}_{21i_1}=\int_{-\mathrm{h}/2}^{\mathrm{h}/2}\mathrm{Q}_{\bar{z}}^{(21)}\mathrm{z}^{\mathrm{i}_1}\mathrm{d}z, \tag{A1}$$
$$a_{22i_1}=\int_{-h/2}^{h/2}Q_{\bar{z}}^{(22)}z^{i_1}\mathrm{d}z,\ \mathrm{a}_{66i_1}=\int_{-\mathrm{h}/2}^{\mathrm{h}/2}\mathrm{Q}_{\bar{z}}^{(66)}\mathrm{z}^{\mathrm{i}_1}\mathrm{d}z,\ \mathrm{i}_1=0,1,2,\ \mathrm{a}_{15i_2}=\int_{-\mathrm{h}/2}^{\mathrm{h}/2}\theta_{1z}\mathrm{Q}_{\bar{z}}^{(11)}\mathrm{z}^{\mathrm{i}_2}\mathrm{d}z,$$
$$a_{18i_2}=\int_{-h/2}^{h/2}\theta_{2z}Q_{\bar{z}}^{(12)}z^{i_2}\mathrm{d}z,\ \mathrm{a}_{25i_2}=\int_{-\mathrm{h}/2}^{\mathrm{h}/2}\theta_{1z}\mathrm{Q}_{\bar{z}}^{(21)}\mathrm{z}^{\mathrm{i}_2}\mathrm{d}z,\ \mathrm{a}_{28i_2}=\int_{-\mathrm{h}/2}^{\mathrm{h}/2}\theta_{2z}\mathrm{Q}_{\bar{z}}^{(22)}\mathrm{z}^{\mathrm{i}_2}\mathrm{d}z,$$
$$a_{35i_2}=\int_{-h/2}^{h/2}\theta_{1z}Q_{\bar{z}}^{(66)}z^{i_2}\mathrm{d}z,\ \mathrm{a}_{38i_2}=\int_{-\mathrm{h}/2}^{\mathrm{h}/2}\theta_{2z}\mathrm{Q}_{\bar{z}}^{(66)}\mathrm{z}^{\mathrm{i}_2}\mathrm{d}z,\ \mathrm{i}_2=0,1,\ \hbar=\mathrm{a}_{110}\mathrm{a}_{220}-\mathrm{a}_{120}\mathrm{a}_{210}.$$

$$c_{11} = a_{111}b_{11} + a_{121}b_{21},\ c_{12} = a_{111}b_{12} + a_{121}b_{11},\ c_{13} = a_{111}b_{13} + a_{121}b_{23} + a_{112},$$
$$c_{14} = a_{111}b_{14} + a_{121}b_{24} + a_{122},\ c_{15} = a_{111}b_{15} + a_{121}b_{25} + a_{151},\ c_{18} = a_{111}b_{18} + a_{121}b_{28} + a_{181},$$
$$c_{21} = a_{211}b_{11} + a_{221}b_{21},\ c_{22} = a_{211}b_{12} + a_{221}b_{22},\ c_{23} = a_{211}b_{13} + a_{221}b_{23} + a_{212},$$
$$c_{24} = a_{211}b_{14} + a_{221}b_{24} + a_{222},\ c_{25} = a_{211}b_{15} + a_{221}b_{25} + a_{251},\ c_{28} = a_{211}b_{18} + a_{221}b_{28} + a_{281},$$
$$c_{31} = a_{661}b_{35},\ c_{32} = a_{661}b_{32} + 2a_{662},\ c_{35} = a_{351} - a_{661}b_{35},\ c_{38} = a_{381} - a_{661}b_{38},$$
$$\theta_j = \int_{-h/2}^{h/2}(1 - 4\bar{z}^2)dz = \frac{2h}{3},\ (j = 3, 4)$$

$$\rho^{(1)} = \rho^{(mix)}\int_{-h/2}^{h/2} z^2 dz,\ \rho^{(2)} = \rho^{(mix)}\int_{-h/2}^{h/2} z\theta_{1z}dz,\ \rho^{(3)} = \rho^{(mix)}\int_{-h/2}^{h/2} z\theta_{2z}dz \tag{A2}$$

## Appendix B. .

The parameters $p_{ij}(i = 1, 2, 3, j = 1, 2, ..., 4)$ included in expression (20) are described as

$$p_{11} = m_1^2\{\chi_{31}h[(c_{11} - c_{31})n_1^2 + c_{12}m_1^2] - c_{13}m_1^2 - (c_{14} + c_{32})n_1^2\},$$
$$p_{11}^{nl} = -\frac{64\chi_1 hc_{12}}{3ab}\frac{m_1^3\varsigma}{n_1},\ p_{11}^{t} = -\rho^{(1)}m_1^2,\ p_{12} = m_1(c_{15}m_1^2 + c_{35}n_1^2 + \theta_3),$$
$$p_{12}^{t} = \rho^{(2)}m_1, p_{13} = (c_{18} + c_{38})m_1^2 n_1,\ p_{21}^{nl} = -\frac{64\chi_2 c_{21}h}{3ab}\frac{n_1^3\varsigma}{m_1},\ p_{21}^{t} = -\rho^{(1)}n_1^2,$$
$$p_{21} = n_1^2\{h\chi_{31}[c_{21}n_1^2 + (c_{22} - c_{31})m_1^2] - (c_{32} + c_{23})m_1^2 - c_{24}n_1^2\},$$
$$p_{22} = (c_{25} + c_{35})m_1 n_1^2, p_{23} = n_1(c_{28}n_1^2 + c_{38}m_1^2 + \theta_4),\ p_{23}^{t} = \rho^{(3)}n_1,$$
$$p_{31} = \chi_{31}h\left(\frac{m_1^2}{r_2} + \frac{n_1^2}{r_1}\right),\ p_{32} = 2m_1^2 n_1^2 h(\chi_1 + \chi_2),\ p_{33} = \theta_3 m_1,$$
$$p_{34} = \theta_4 n_1,\ p_{31}^{nl} = -\frac{8h}{3ab}\left[2\left(\frac{\chi_1}{r_2}\frac{m_1}{n_1} + \frac{\chi_2}{r_1}\frac{n_1}{m_1}\right) + m_1 n_1\chi_{31}\right]\varsigma,$$
$$\varsigma = [1 - (-1)^m - (-1)^n + (-1)^{m+n}]. \tag{B1}$$

## References


[1] Iijima S. Helical microtubules of graphitic carbon. Nature 1991;354:56–8.
[2] Iijima S, Ichihashi T. Single-shell carbon nanotubes of 1-Nm diameter. Nature 1993;363:603–5.
[3] Trovalusci P, Augusti G. A continuum model with microstructure for materials with flaws and inclusions. J Phys IV France 1998; 08 (PR8) Pr8-383-Pr8-390.
[4] Xie S, Li W, Pan Z, Chang B, Sun L. Mechanical and physical properties on carbon nanotube. J Phys Chem Solids 2000;61(7):1153–8.
[5] Dresselhaus MS, Dresselhaus G, Eklund PC. Science of Fullerenes and Carbon Nanotubes. New York: Academic Press; 1996.
[6] Fantuzzi N, Bacciocchi M, Agnelli J, Benedetti D. Three-phase homogenization procedure for woven fabric composites reinforced by carbon nanotubes in thermal environment. Compos Struct 2020;254:112840.
[7] Tuna M, Kirca M, Trovalusci P. Deformation of atomic models and their equivalent continuum counterparts using Eringen's two-phase local/nonlocal model. Mech Res Communicat 2019;97:26–32.
[8] Izadi R, Tuna M, Trovalusci P, Ghavanloo E. Torsional characteristics of carbon nanotubes: micropolar elasticity models and molecular dynamics simulation. Nanomaterials 2021;11:453.
[9] Jin FL, Park SJ. Recent Advances in carbon-nanotube-based epoxy composites. Carbon Letters 2013;1:1–13.
[10] Aravand M, Lomov SV, Verpoest I, Gorbatikh L. Evolution of carbon nanotube dispersion in preparation of epoxy-based composites: From a masterbatch to a nanocomposite. eXPRESS Polym Lett 2014;8:596–608.
[11] Tjong SC. Polymer Composites with Carbonaceous Nanofillers Properties and Applications. KGaA: Wiley-VCH Verlag GmbH & Co; 2012.
[12] Ren Z, Lan Y, Wang Y. Aligned Carbon Nanotubes: Physics, Concepts, Fabrication and Devices. Berlin-Heidelberg: Springer Verlag; 2013.
[13] Shen HS, Xiang Y. Nonlinear vibration of nanotube-reinforced composite cylindrical shells in thermal environments. Comput Methods Appl Mech Eng 2012; 213:196–205.
[14] Pouresmaeeli S, Fazelzadeh S. Frequency analysis of doubly curved functionally graded carbon nanotube-reinforced composite panels. Acta Mech 2016;227: 2765–94.
[15] Mehar K, Panda SK. Nonlinear finite element solutions of thermoelastic flexural strength and stress values of temperature dependent graded CNT-reinforced sandwich shallow shell structure. Struct Eng Mech 2018;67(6):565–678.
[16] Ansari R, Torabi J, Hassani RA. comprehensive study on the free vibration of arbitrary shaped thick functionally graded CNT-reinforced composite plates. Eng Struct 2019;181:653–69.
[17] Bacciocchi M, Luciano R, Majorana R, Tarantino AM. Free vibrations of sandwich plates with damaged soft-core and non-uniform mechanical properties: Modeling and finite element analysis. Materials 2019;12:2444.
[18] Bacciocchi M, Luciano R, Majorana R, Tarantino AM. Natural frequency analysis of functionally graded orthotropic cross-ply plates based on the finite element method. Math Computat Appl 2019;24(52):1–21.
[19] Avey M, Yusufoglu E. On the solution of large-amplitude vibration of carbon nanotube-based doubly curved shallow shells. Math Meth Appl Sci 2020:1–12. https://doi.org/10.1002/mma.6820.
[20] Wang A, Chen H, Zhang W. Nonlinear transient response of doubly curved shallow shells reinforced with graphene nanoplatelets subjected to blast loads considering thermal effects. Compos Struct 2019;225:111063.
[21] Qin Z, Zhao S, Pang X, Safaei B, Fulei C. A unified solution for vibration analysis of laminated functionally graded shallow shells reinforced by graphene with general boundary conditions. Int J Mech Sci 2020;170:105341.
[22] Bisheh H, Wu N, Rabczuk T. Free vibration analysis of smart laminated carbon nanotube-reinforced composite cylindrical shells with various boundary conditions in hygrothermal environments. Thin-Walled Struct 2020;149:106500.
[23] Tocci Monaco G, Fantuzzi N, Fabbrocino F, Luciano R. Hygro-thermal vibrations and buckling of laminated nanoplates via nonlocal strain gradient theory. Compos Struct 2021;262:113337.
[24] Tham VV, Tran HQ, Tu TM. Vibration characteristics of piezoelectric functionally graded carbon nanotube-reinforced composite doubly-curved shells. Appl Math Mech (Eng Edit) 2021;42(6):819–40.
[25] Deniz A, Fantuzzi N, Sofiyev AH, Kuruoglu N. Modeling and solution of large amplitude vibration problem of construction elements made of nanocomposites using shear deformation theory. Materials 2021;14:3843.
[26] Pasternak PL. On a new method of analysis of an elastic foundation by means of two foundation constants. State Pub House Lit Constr Archit, Moscow 1954;1:1–56 [in Russian].
[27] Kerr AD. Elastic and viscoelastic foundation models. J Appl Mech 1964;31:491–8.

[28] Tornabene F, Fantuzzi N, Viola E, Reddy JN. Winkler-Pasternak foundation effect on the static and dynamic analyses of laminated doubly-curved and degenerate shells and panels. Compos Part B-Eng 2014;57:269–96.
[29] Zhang LW, Liew KM. Large deflection analysis of FG-CNT reinforced composite skew plates resting on Pasternak foundations using an element-free approach. Compos Struct 2015;132:974–93.
[30] Ansari R, Torabi J, Shojaei M. Faghih Vibrational analysis of functionally graded carbon nanotube-reinforced composite spherical shells resting on elastic foundation using the variational differential quadrature method. Euro J Mech A-Solids 2016;60:166–82.
[31] Dinh DC, Nguyen PD. The dynamic response and vibration of functionally graded carbon nanotube-reinforced composite (FG-CNTRC) truncated conical shells resting on elastic foundations. Materials 2017;10(10):1194.
[32] Shen HS, He XQ. Large amplitude free vibration of nanotube-reinforced composite doubly curved panels resting on elastic foundations in thermal environments. J Vib Control 2017;23(16):2672–89.
[33] Babaei H, Kiani Y, Eslami MR. Large amplitude free vibration analysis of shear deformable FGM shallow arches on nonlinear elastic foundation. Thin-Wall Struct 2019;144:106237.
[34] Sobhy M, Zenkour AM. Vibration analysis of functionally graded graphene platelet reinforced composite doubly-curved shallow shells on elastic foundations. Steel Compos Struct 2019;133(2):195–208.
[35] Vu NVH, Nguyen DT, Dinh GN. Nonlinear dynamics of functionally graded graphene nanoplatelet reinforced polymer doubly-curved shallow shells resting on elastic foundation using a micromechanical model. J Sand Struct Mater 2020: 1099636220926650.
[36] Sofiyev AH, Pirmamedov IT, Kuruoglu N. Influence of elastic foundations and carbon nanotube reinforcement on the hydrostatic buckling pressure of truncated conical shells. Appl Math Mech (Eng Edit) 2020;41(7):1011–26.
[37] Sofiyev AH, Kuruoglu N. Buckling analysis of shear deformable composite conical shells reinforced by CNTs subjected to combined loading on the two-parameter elastic foundation. Defence Techn 2021:1–14. https://doi.org/10.1016/j.dt.2020.12.007 (in press).
[38] Zhang Y, Zhang B, Shen H, Wang Y, Liu J. Nonlinear bending analysis of functionally graded CNT-reinforced shallow arches placed on elastic foundations. Acta Mech Solid Sinica 2020;33(2):164–86.
[39] Ambartsumian SA. Theory of Anisotropic Shells, NASA. TT F-118 1964.
[40] Amabili M. Nonlinear Vibrations and Stability of Shells and Plates. New York: Cambridge University Press; 2008.
[41] Amabili M. A new third-order shear deformation theory with non-linearities in shear for static and dynamic analysis of laminated doubly curved shells. Compos Struct 2015;128:260–73.
[42] Amabili M, Païdoussis MP. Review of studies on geometrically nonlinear vibrations and dynamics of circular cylindrical shells and panels, with and without fluid-structure interaction. Appl Mech Rev 2003;56 (4): 349–381.
[43] Volmir AS. Nonlinear Dynamics of Plates and Shells. Moscow: Nauka; 1972.
[44] Amabili M. Non-linear vibrations of doubly curved shallow shells. Int J Nonlin Mech 2005;40:683–710.
[45] Alijani F, Amabili M, Karagiozis K, Bakhtiari-Nejad F. Nonlinear vibrations of functionally graded doubly curved shallow shells. J. Sound Vib 2011;330(7): 1432–54.
[46] Sofiyev AH. On the vibration and stability behaviors of heterogeneous-CNTRC-truncated conical shells under axial load in the context of FSDT. Thin-Walled Struct 2020;151:106747.
[47] Grigolyuk EI. On vibrations of a shallow circular cylindrical panel experiencing finite deflections. Appl Math Mech 1955;19(3): 386-382.